JOURNAL OF GEOPHYSICAL RESEARCH, VOL. 113, E08004, doi:10.1029/2007JE002992, 2008

Mechanisms of faulting in and around Caloris basin, Mercury

Patrick J. Kennedy,[1] Andrew M. Freed,[1] and Sean C. Solomon[2]

Received 16 August 2007; revised 3 March 2008; accepted 2 April 2008; published 7 August 2008.

[1] The distribution of faulting in and around the Caloris basin on Mercury provides constraints on the planet's early lithosphere and tectonic history. By means of a series of finite element models we test a range of ideas regarding lithospheric structure, surface loading, and shallow flow proposed to account for early contractional features and younger extensional features on the basin floor as well as contractional tectonic features exterior to the basin. Early-stage thrust faults within the basin are well matched by the stress field accompanying flexural subsidence in response to partial infilling of a broad basin floor, while younger normal faulting can be the result of flexural uplift in response to later-stage emplacement of an exterior annulus of smooth plains deposits. A proposed scenario in which later-stage inward flow of the lower crust induces uplift of the basin floor can, under some conditions, yield extension in the basin, but not in a manner consistent with the observed distribution of normal faults. Thrust faulting on the exterior smooth plains can be the result of local subsidence accompanying the emplacement of these units but may also have been influenced by global contraction. Our results lead to the prediction that the gravity anomaly associated with the Caloris basin and surroundings should consist of a central positive anomaly (mascon) and an annular gravity high separated by a ring of lower gravity. Gravity and topography measurements to be made by the MESSENGER mission will provide a test of this prediction and more generally of the models developed here.

Citation: Kennedy, P. J., A. M. Freed, and S. C. Solomon (2008), Mechanisms of faulting in and around Caloris basin, Mercury, *J. Geophys. Res.*, *113*, E08004, doi:10.1029/2007JE002992.

1. Introduction

[2] An important aspect of the early evolution of a terrestrial planet is the thermal and mechanical development of the lithosphere, as revealed by its response to various forms of loading. Whereas the evidence regarding the nature of the early lithosphere has long since been removed on Earth and Venus, Mercury's heavily cratered surface appears to have experienced comparatively little volcanic resurfacing or tectonic activity since the end of heavy bombardment (~3.8 Ga) [*Spudis and Guest*, 1988; *Solomon*, 2003]. The Caloris basin, at 1300 km in diameter [*Pike*, 1988] one of the largest and youngest impact basins on Mercury, preserves an extensive pattern of faulting that provides important clues to the manner by which Mercury's early lithosphere responded to basin formation and to subsequent lithospheric loading. Unraveling the processes that led to faulting in and around the Caloris basin can provide insight into the early tectonic history of the planet.

[3] A variety of faulting styles are observed within and exterior to the half of the Caloris basin imaged by Mariner 10 (Figure 1). Inside the basin, extensional graben are observed to crosscut contractional ridges, indicating at least two phases of faulting, while outside the basin contractional ridges are the dominant fault form [*Strom et al.*, 1975]. Whereas contractional features inside the basin likely resulted from subsidence associated with partial infilling of the basin by volcanic deposits, the process that led to the subsequent development of extensional features is not clear. Three suggestions have been proposed: uplift as a result of continued isostatic readjustment to basin formation [*Dzurisin*, 1978; *Melosh and Dzurisin*, 1978], uplift caused by exterior volcanic loading [*McKinnon*, 1980; *Melosh and McKinnon*, 1988], and uplift induced by inward flow of the lower crust [*Watters et al.*, 2005]. Contractional features outside the basin may have resulted from subsidence associated with the placement of an annular load outside the basin [*Melosh and McKinnon*, 1988], perhaps augmented by compressional stresses accompanying global contraction [*Strom et al.*, 1975]. It is also notable that exterior circumferential graben, such as those observed around most mascon mare basins on the Moon, are absent from the Caloris basin. Whether this absence is the result of covering by younger deposits or because such features never formed is not presently known.

[4] The style and distribution of faulting in and around the Caloris basin can be applied as constraints on numerical simulations of the response of Mercury's lithosphere to an evolving combination of volcanic and global contractional loading. Here we use axisymmetric viscoelastic models to

[1]Department of Earth and Atmospheric Sciences, Purdue University, West Lafayette, Indiana, USA.
[2]Department of Terrestrial Magnetism, Carnegie Institution of Washington, Washington, DC, USA.

0148-0227/08/2007JE002992$09.00

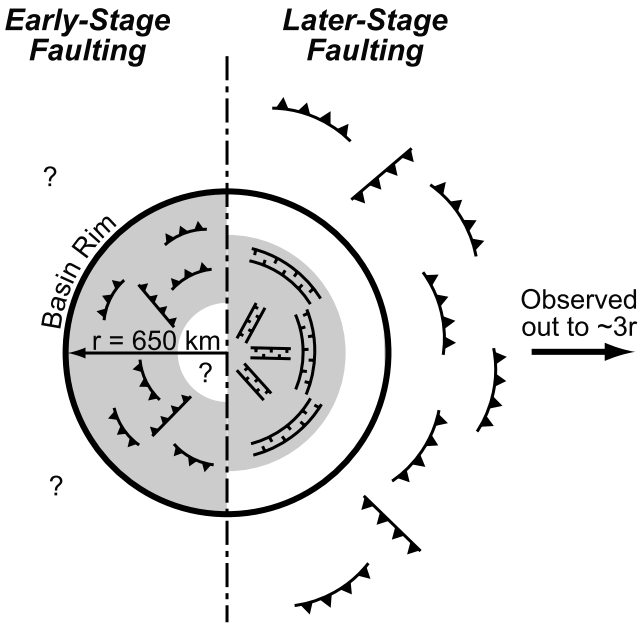

Figure 1. Schematic summary of faulting observed in and around the eastern half of the Caloris basin imaged by Mariner 10 and during the January 2008 flyby of Mercury by MESSENGER. The general locations of contractional features (scarps, ridges) are shown by barbed lines, while extensional features (troughs, graben) are shown by hachured lines. The left-hand side shows an early stage of interior basin faulting (still for the eastern basin half) that was crosscut by the faulting shown on the right-hand side (also for the eastern basin half). Early stage contractional features are found throughout the basin floor (grey region on left-hand side) [*Strom et al.*, 1975], although the nature of thrust faulting within the innermost 200 km has not yet been determined. Later-stage extensional features within the basin are primarily found within ~470 km of the basin center (grey region on right-hand side) [*Watters et al.*, 2005; *Murchie et al.*, 2008]. The contractional features exterior to the basin occur in part on smooth plains units that are less cratered and therefore younger than the smooth plains on the Caloris basin floor [*Spudis and Guest*, 1988]. These external faults are therefore shown in this figure as "later-stage," but the relative timing of exterior contractional features and interior extensional features is poorly constrained.

understand how styles of faulting are influenced by assumptions regarding the shape of the Caloris basin floor, the magnitude of interior and exterior loads, the thickness of the lithosphere, the strength of surface rocks, and the viscosity structure of the interior. We also test two of the mechanisms proposed to explain late-stage extensional features on the Caloris basin floor.

[5] This analysis is motivated not only by an interest in unraveling the early tectonic history of Mercury, but also to predict what might be found during observations of Mercury to be made by the MESSENGER (MErcury Surface, Space ENvironment, GEochemistry, and Ranging) spacecraft [*Solomon et al.*, 2001, 2007]. Launched in 2004, MESSENGER flew by Mercury in January 2008 and will do so again in October 2008 and September 2009. MESSENGER is scheduled to be inserted into orbit about Mercury in March 2011. The spacecraft carries a suite of seven instruments plus a radio science investigation. Most central to the topic of this paper are an imaging system that will provide color and higher-resolution monochrome images of the entire planet as well as stereo images for topography, a laser altimeter that will produce topographic maps of the northern hemisphere, and the radio science investigation, which will yield a planetary gravity field. Also relevant are geochemical and mineralogical remote sensing instruments that will help constrain crustal composition and volcanic history and a magnetometer that may detect crustal magnetic anomalies pertinent to the planet's thermal and magmatic history.

2. Observational Constraints

[6] The floor of the Caloris basin is covered with smooth plains, interpreted to result from the extrusion of volcanic material somewhat after basin formation [*Strom et al.*, 1975; *Spudis and Guest*, 1988]. These plains are extensively fractured. Contractional ridges are found with both basin-concentric and basin-radial orientations over much of the basin floor, most prominently in an arc extending from ~430 to ~600 km from the basin center (Figure 1) [*Strom et al.*, 1975]. Fault patterns in the innermost regions of the Caloris floor were not determined by Mariner 10, because at the time of those flybys the dawn terminator was approximately 200 km east of the basin center and the central basin floor was not illuminated. MESSENGER imaged the entire Caloris basin during its January 2008 flyby [*Murchie et al.*, 2008], albeit at high Sun angles not ideal for the identification of low-relief tectonic features. The ridges within Caloris are considered analogous to those found within lunar mascon mare basins, which formed when uncompensated mare basalt fill induced lithospheric subsidence that resulted in horizontal compressional stresses, contractional strain, and near-surface faulting. At some point, the stress state within the Caloris basin changed from compressional to extensional, as numerous extensional troughs crosscut the ridges and are therefore younger (Figure 1) [*Strom et al.*, 1975; *Dzurisin*, 1978; *Melosh and McKinnon*, 1988]. These troughs have been interpreted to be graben as much as 10 km wide [*Watters et al.*, 2005]. The graben imaged by Mariner 10 are concentrated in a broad arc that extends from at least ~200 to ~470 km from the basin center [*Watters et al.*, 2005], and although they display both basin-concentric and basin-radial trends, they are predominantly basin-concentric in this region [*Dzurisin*, 1978; *Pechman*, 1980]. During its January 2008 flyby, MESSENGER imaged graben in the central region of the Caloris basin, but those features display basin-radial trends [*Murchie et al.*, 2008]. None of these later-stage extensional features are observed in lunar mascon mare basins or basins on other terrestrial planets.

[7] The region outside the Caloris basin is covered by hummocky plains, interpreted to be ejecta, and more extensive smooth plains, interpreted to be either fluidized impact ejecta or volcanic deposits. A volcanic source is favored,

because the estimated volume (5×10^7 km^3) is far in excess of the amount of impact melt to be expected from an impact basin the size of Caloris [*Head*, 1974; *Strom et al.*, 1975]. In addition, crater densities show that the smooth plains significantly postdate the ejecta blanket and were emplaced over an extended period of time [*Strom*, 1984; *Spudis and Guest*, 1988]. While the hummocky plains are observed just outside the basin rim, the smooth plains appear to begin 100–200 km outward of the basin rim and extend as far as ~3 basin radii [*Strom et al.*, 1975].

[8] The exterior plains are extensively cut by contractional features (wrinkle ridges and scarps) oriented both radially and concentric to the basin rim (Figure 1) [*Strom et al.*, 1975], though most such tectonic features are basin-concentric [*Dzurisin*, 1978]. Such contractional features are also observed around lunar mascon basins in the form of mare ridges [*Phillips et al.*, 1972; *Solomon and Head*, 1979, 1980; *Freed et al.*, 2001]. Basin-concentric wrinkle ridges well outside the impact basin on the Moon are thought to represent a response to some combination of basin loading at a time when cooling of the mantle had led to a thicker (>100 km) mechanical lithosphere and superposed compressive stress from global contraction [*Phillips et al.*, 1972; *Solomon and Head*, 1979, 1980; *Freed et al.*, 2001]. Plains external to the Caloris basin, however, may have themselves exerted a strong influence on local or regional flexure if emplaced in deposits of sufficient thickness [*Melosh and McKinnon*, 1988], as suggested by topographic profiles across low-latitude exterior plains units obtained by Earth-based radar [*Harmon et al.*, 1986]. A contribution from global contraction may also have been important.

[9] The relative timing of deformation internal and external to the Caloris basin rim is not well constrained, inasmuch as the deformational features of the two regions do not intersect. Large areas of the exterior annulus of smooth plains appear to be less heavily cratered and therefore younger than the smooth plains on the Caloris basin floor [*Spudis and Guest*, 1988], so on that basis the surface expressions of contractional features exterior to the basin are likely to be somewhat younger than the contractional features on the basin-filling plains. We depict the exterior contractional features in Figure 1 as more nearly contemporaneous with the interior graben than with the interior contractional strain, but such an assignment is not a certain one.

3. Proposed Mechanisms of Graben Formation

[10] Three mechanisms for later-stage graben formation in the interior of the Caloris basin have been suggested. The earliest suggestion was that the uplift was the result of isostatic readjustment to basin excavation [*Dzurisin*, 1978; *Melosh and Dzurisin*, 1978]. By such a hypothesis, rebound toward an isostatic state occurred on a substantially longer timescale than the duration of smooth plains emplacement on the basin floor. Such a scenario is at variance, however, with the timescale for isostatic rebound on the modern Earth (thousands to tens of thousands of years [e.g., *Peltier*, 2004]) versus that for mare volcanism within impact basins on the Moon (hundreds of millions of years [e.g., *Solomon and Head*, 1980]). The viscosity of Mercury's upper mantle need not be identical to that of Earth today, of course, but any readjustment for basin excavation would have been at the end of the era of heavy bombardment and would have in particular been concentrated beneath the newly formed basin itself, where impact heating would have accelerated mantle flow. The timescale for partial volcanic infilling of the Caloris floor also need not have matched that for the lunar mascon maria, but the difference in crater density between floor material and basin material [*Spudis and Guest*, 1988] indicates a delay between basin excavation and cessation of floor volcanism and supports an extended time frame for infilling. We do not consider this hypothesis for floor uplift further, although a variant of the hypothesis in which an isostatic state for the basin was rapidly achieved but inward flow of the lower crust and consequent uplift of the basin floor continued over a much longer timescale is described below.

[11] A second hypothesis for later-stage graben formation is that the exterior smooth plains exerted an annular load on Mercury's lithosphere that induced subsidence and compression exterior to the basin and flexural uplift and extension in the basin interior [*McKinnon*, 1980; *Melosh and McKinnon*, 1988]. This hypothesis built on the proposal by *Melosh and Dzurisin* [1978], motivated by the proximity of the longitude of Caloris to that of one of Mercury's "hot poles" that face the Sun at Mercury perihelion, that the exterior smooth plains deposits constitute an excess mass detectable as an annular positive gravity anomaly. An analytical calculation using the thick-plate flexure theory of *Melosh* [1978] showed that an annular 400-m-thick load from 650 to 1800 km (1 to ~3 basin radii) radial distance from the basin center would be sufficient to induce circumferential normal faulting within the basin, provided that the lithosphere was between 75 and 125 km thick at the time of loading [*McKinnon*, 1986].

[12] A key to this idea is that the emplacement of most of the exterior annular load occurred after subsidence induced by basin fill had run essentially to completion, in order that extensional graben generally crosscut ridges in the basin interior. The analytical modeling of this scenario is based on the assumption that at the time of emplacement of the external load, the basin and its fill were isostatically compensated and the stress state of the basin fill was hydrostatic. However, a common assumption in modeling the basin-related stress field is that the impact leaves a freshly excavated basin that rapidly achieves an isostatic state and then is partially filled by uncompensated volcanic units, leading to subsidence and compressive flexural stresses, as evidenced by the ridges that formed within the basin. Though thrust faulting would have relieved some portion of the compressional state of the fill, it is likely that the fill would remain in a state of compression. Thus in order for a flexural response to an annular ring load to generate extensional stresses within the basin, the load must be sufficient to overcome residual compressional stresses. This factor has not been previously considered in modeling.

[13] A third hypothesis for a younger episode of graben formation within the Caloris basin [*Watters et al.*, 2005] posits that a later-stage of basin uplift and extensional strain accompanied inward flow at the base of regionally thick crust. In this scenario, which is independent of the nature and timing of basin-exterior smooth plains, at the cessation

of partial volcanic infilling, basin subsidence, and wrinkle ridge formation, the crust beneath the basin remained thinner than beneath the surrounding regions. The lateral variation in crustal thickness gave rise to horizontal pressure gradients that drove flow of the lowermost crust toward the basin interior. This flow produced uplift of the basin floor, generated extensional stresses, and led to normal faulting.

[14] As with the hypothesis of an external annular load, previous modeling associated with the lower crustal flow scenario [*Watters et al.*, 2005] began with the assumption of an isostatically compensated basin with a hydrostatic stress state. Those models did not consider the need to overcome residual compressive stresses required to account for the older ridges. Moreover, the lower crustal flow modeling did not treat the response of a hotter and possibly weaker asthenosphere that certainly responded to initial basin excavation and loading and would also have reacted to any inward transport of crustal material. Here we distinguish rapid asthenospheric flow in the mantle from slower viscous flow in the lower crust. A strong uppermost mantle layer may or may not have been present between the lower crust and the asthenosphere. In particular, this scenario requires that the lower crust was sufficiently strong to have avoided significant flow during initial basin subsidence and associated asthenospheric flow but instead flowed inward over a markedly longer timescale. If, however, basin fill was emplaced in stages over tens to hundreds of millions of years as, for example, inferred for the loading of mascon mare basins on the Moon [e.g., *Solomon and Head*, 1980], then the timescales for asthenospheric flow and lower crustal channel flow may have overlapped.

4. Modeling Approach

[15] Our modeling objective is to find a self-consistent model stress history that can explain the formation of ridges in the interior of the Caloris basin, circumferential graben that crosscut the ridges, and predominantly concentric ridges on the exterior plains. Our approach is to develop spherical, axisymmetric finite element models that can simulate basin and crust-mantle boundary geometry, time-dependent loading processes, and the relaxation of a viscoelastic lower crust and mantle and from which near-surface stresses may be calculated to predict faulting styles for comparison with observations. We utilize the finite element code TEKTON [*Melosh and Raefsky*, 1980] because of its large-strain capability and for ease of comparison with a parallel study of lunar mascon basins [*Freed et al.*, 2001].

[16] Relatively little is known regarding the shape of the Caloris basin beneath the fill (and therefore the thickness of the fill), although we note that photoclinometric analysis of Mariner 10 images yielded an estimate for relief between the Caloris basin rim and center of 9 ± 3 km [*Hapke et al.*, 1975]. Here we make use of the inferred geometry of mare basalt fill in the lunar mascon basin Imbrium as a proxy, as it is close in diameter to Caloris and also dates from near the end of heavy bombardment. The thickness of Imbrium basin fill was estimated by *Solomon and Head* [1980] to be 9 km at its center on the basis of the magnitude of a typical mascon gravity anomaly and a scaling of the prefill topographic profile from that of the Orientale basin, obtained at that time from limb height observations. The thickness of mare basalt fill in the center of the Imbrium basin was estimated more recently at 5 km on the basis of global altimetry obtained from the Clementine mission and a basin depth-diameter relation for unfilled basins [*Williams and Zuber*, 1998], although loading-induced subsidence during basin infilling was not considered in the derivation of that estimate. Because surface gravitational attraction on Mercury is more than twice that of the Moon, to the extent that basin relief is limited by gravitationally induced stress differences the depth of a basin on Mercury should be less than on the Moon for a given size feature. On the basis of all of these considerations, we adopt a fill thickness for the central Caloris basin of 5 km, but we recognize that this figure has considerable uncertainty. We consider two basin floor profiles, one that shoals rapidly with distance from its center (Figure 2, inset) and is scaled from the profile for the Imbrium basin given by *Solomon and Head* [1980], and one where the basin floor geometry remains flat farther out from the basin center (i.e., displays a broader region of thick fill). We also consider the possibility that the basin was not filled in one stage, but in several. In a simple representation of multistage filling, we a consider a model in which subsidence following an initial 4-km-thick fill was completed before an uppermost 1 km of basalt was emplaced. This extended infilling sequence has the effect that the uppermost layer experiences stresses associated only with its own subsidence and subsequent processes.

[17] The spherical, axisymmetric finite element model of the Caloris basin and surrounding region used in our study is shown in Figure 2. Tests of different meshes show that further refinement of element size does not significantly influence model results. Model curvature is associated with a planet radius of 2440 km. The model extends to a depth of 400 km, and the circumference is 7665 km, about half the circumference of Mercury. Thus we have modeled the response of the entire planet to Caloris processes. The side and bottom boundaries are fixed, except for the axis of symmetry, along which nodes are allowed to displace in the vertical direction. An intervening asthenosphere prevents the fixed bottom boundary from influencing results, and the far-field lateral boundary is beyond the reach of either the basin or external annular loads. We assume a crustal density of $\rho_c = 2900$ kg/m^3 and a mantle density of $\rho_m = 3300$ kg/m^3. Both the interior and exterior smooth plains associated with the Caloris basin lack a strong albedo contrast with rest of the surface, suggesting that the plains composition is likely similar to that of the rest of the crust and has much lower abundances of iron and titanium than most lunar mare basalts [*Hapke et al.*, 1975]. We thus assume that interior and exterior fill have a density similar to that of the crust, $\rho_f = 2900$ kg/m^3. We take the elastic strength of Mercury's lithosphere to be uniform, with Young's modulus $E = 10^{11}$ Pa and Poisson's ratio $\nu = 0.25$. Mercury's surface gravitational attraction is 3.76 m/s^2.

[18] As the thickness of the mechanical lithosphere early in Mercury's history is relatively unconstrained, we consider thicknesses of 50, 120, and 200 km. Modeled crustal thickness (we assumed 50 km) does not significantly influence results except in the lower crustal flow scenario, where we assume a 120-km-thick crust as suggested by *Watters et al.* [2005], who inferred that a sufficiently low viscosity would not be encountered in crustal material

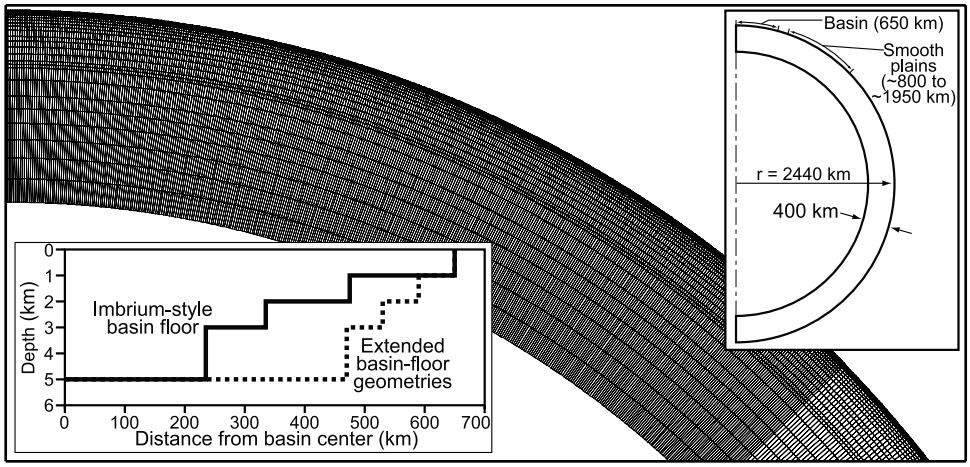

Figure 2. Axisymmetric finite element model used to study the response of Mercury's lithosphere and asthenosphere to loading in and around the Caloris basin. The main frame shows in detail a portion of the model around the basin and smooth plains region. The inset at upper right shows the geometry of the full model, which by symmetry includes the outer layers of the entire planet; a global model is required because of the far reach of the loads associated with the exterior smooth plains. The inset at lower left shows the two basin floor geometries considered in the analysis. The Imbrium-scaled basin floor is based on the inferred geometry of the similar sized Imbrium basin on the Moon, while the extended basin floor geometries enable basin fill to remain uniformly thicker much farther from the basin center. Note the vertical exaggeration of 190:1 in this inset.

shallower than about 50 km for a dry anorthite rheology and who invoked estimates of the depth of the brittle-ductile transition constrained by topographic profiles across lobate scarps [*Nimmo and Watters*, 2004]. This assumption of a relatively thick crust maximizes the thickness of a viscoelastic lower crustal channel.

[19] The thickness of the annular smooth plains deposits, which extend approximately 2 basin radii from the basin rim, is not well constrained. From estimates for the amount of material necessary to fill surrounding basins, *Strom et al.* [1975] suggested that the smooth plains material could be as thick as 10 km. However, an average smooth plains thickness of less than 1 km was derived from analyses of the depths of partially filled craters [*DeHon*, 1979; *Kiefer and Murray*, 1987]. Here we consider thicknesses of 1, 5, and 10 km. As smooth plains are inferred to be sparse for the first 100–200 km outside the basin rim, we model these plains as extending from 750 to 1800 km from the basin center, with the first 100 km and last 300 km linearly tapered to zero thickness. Regardless of the assumed load thickness, the plains are modeled with a 1-km thick row of elements with the density (nominally 2900 kg/m^3) adjusted to generate the desired load.

[20] Although the viscosity of the asthenosphere at the time of basin subsidence and subsequent extension is not known, we may assume that this region has long since completely relaxed. Thus the assumed viscosity (we chose 10^{18} Pa s) is not important as long as a completely relaxed state is achieved. The asthenosphere is assumed to extend to the 400-km-deep base of the model. The lower crustal flow scenario requires that the asthenosphere be relaxed (i.e., initial basin subsidence be complete) prior to later-stage lower crustal flow. To simulate this scenario, TEKTON allows us to model the lower crust as elastic until the asthenosphere completely relaxes in response to basin fill, and then switch the viscosity of the lower crust to be 10^{18} Pa s, enabling later-stage flow. This evolutionary sequence produces a result equivalent to modeling the lower crust with a much higher viscosity than the asthenosphere but enables much shorter calculation times. The upper crust and lithospheric mantle (where present) are assumed to be elastic throughout all calculations.

[21] For each of the loading scenarios we assume that the basin formation process left an initially unfilled Caloris basin that was isostatically compensated, i.e., a hydrostatic stress state in which all normal stresses are equal to the overburden and shear stresses are minimal. To begin the calculation in a state of hydrostatic stress, surface topography must be supported by either variations in crustal thickness (Airy isostasy) or variations in crustal density (Pratt isostasy). Because isostatic compensation induces horizontal pressure gradients that can drive viscoelastic flow at depths greater than the brittle-ductile transition, in our model the compensation must be shallower than the depth of the shallowest region displaying viscoelastic behavior or compensation will not be maintained and spurious stresses will be generated. We therefore model isostatic compensation in two ways. If the lithosphere is thicker than the crust, we deflect the crust-mantle boundary upwards beneath the basin to establish Airy compensation. If the lithosphere is thinner than the crust, we reduce crustal densities above the brittle-ductile transition to establish Pratt compensation. We find that the means of compensation does not significantly influence the outcome of a given loading scenario. To calculate the initial hydrostatic stress state, the density and stiffness of elements that will eventually represent basin and smooth plains fill are removed. Overburden stresses are calculated by applying gravity, and those stresses are then imported back into the model as prestresses in the three principal stress directions. The

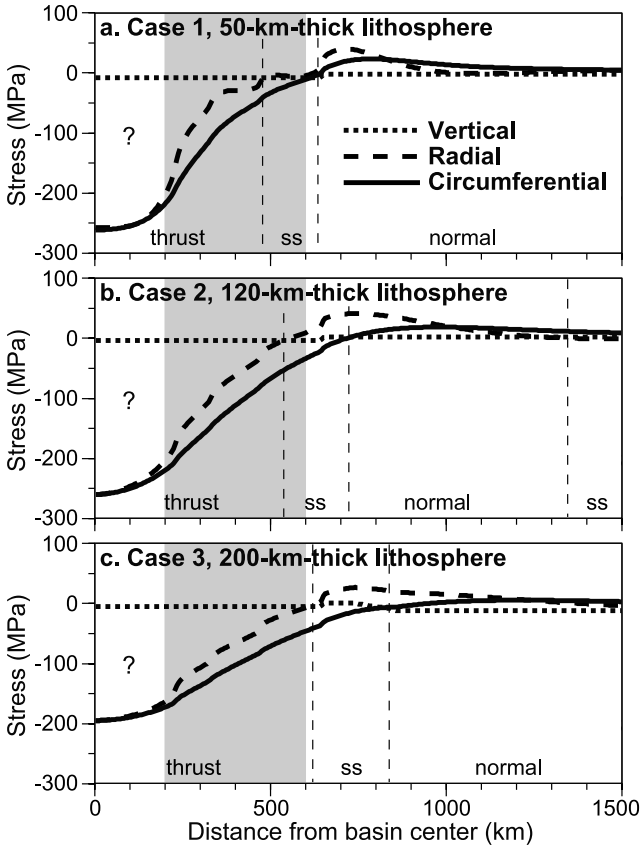

Figure 3. Principal stresses as functions of distance from the center of Caloris after partial basin infilling and subsidence for a basin floor geometry scaled from that of the lunar Imbrium basin. Case numbers refer to Table 1. Negative stresses are compressive. Principal stresses are shown for the center of the uppermost elements in the model. At this shallow depth (within 0.5 km of the surface), the three principal stress directions can be well approximated by vertical, basin radial, and basin circumferential. Flexural stresses have been calculated by subtracting the initial isostatic stress state. The gray region shows where early-stage thrust faulting in the Caloris basin is observed. The question mark in the innermost basin denotes that the nature of thrust faulting within this region is not known.

process is repeated several times until the application of gravity no longer induces significant displacements or differential stresses.

[22] Predicted faulting styles are calculated according to the criterion of *Anderson* [1951], which prescribes the style of faulting on the basis of whether the vertical stress is the least compressive (thrust faulting), intermediate (strike-slip faulting), or most compressive (normal faulting) principal stress. When the radial stress is more compressive than the circumferential (hoop) stress, thrust faults are concentrically oriented and normal faults are radially oriented with respect to the basin.

[23] The analysis simulates three loading processes: that associated with early infilling of the Caloris basin by smooth plains material and consequent subsidence, that associated with later emplacement of the exterior smooth plains, and that associated with lower crustal flow following initial subsidence. Each loading scenario begins with an isostatically compensated, unfilled Caloris basin; then uncompensated basin fill material is added, and the asthenosphere is allowed to relax fully. Thereafter either the lower crust is allowed to flow or a load exterior to the basin is applied. Each model leads to predictions of stresses in the upper crust, faulting styles, and proximity to failure. Our goal is to find the combination of loading scenarios and model parameters that leads to predictions of faulting that are most consistent with observations.

5. Subsidence of Caloris Due to Basin Fill

[24] The model configurations considered in our effort to understand the development of thrust faults within the Caloris basin are summarized in Table 1. We initially model subsidence due to Caloris basin fill with an Imbrium-scaled floor geometry and a range of lithospheric thicknesses (cases 1, 2, and 3 in Table 1). Figures 3a, 3b, and 3c show the predicted stress state after the initial isostatic stress state has been subtracted (to illuminate flexural stresses) near the surface (top row of elements) for models with a lithospheric thickness of 50, 120, and 200 km, respectively. On these panels the predicted style of faulting near the surface is noted as a function of distance from the basin center. Predicted styles of faulting are shown to a depth of 20 km in the crust in Figures 4a, 4b, and 4c for these same cases. Figure 4 demonstrates that faulting styles generally do not vary within the top 10 km of the crust, and usually not within the top 20 km, well within the depth range that basin-related faults are likely to initiate (a few kilometers). Thus

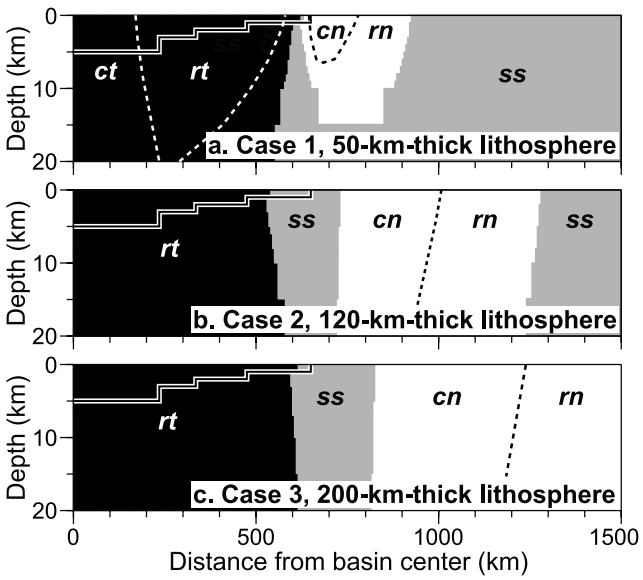

Figure 4. Predicted styles of faulting as functions of distance from the center of the Caloris basin associated with subsidence of uncompensated basin fill for a basin floor geometry scaled from that of the lunar Imbrium basin. Case numbers refer to Table 1. Basin floor geometry is shown as a black-on-white line. Styles of faulting: ct, concentric thrust; rt, radial thrust; ss, strike-slip; cn, concentric normal; rn, radial normal. Model curvature associated with planetary curvature is not shown.

Table 1. Models for Early-Stage Thrust Faulting Within the Caloris Basin[a]

Case	Caloris Basin Floor Geometry	Interior Fill Thickness at Center, km	Lithospheric Thickness, km	Interior Thrust faults?	Smallest Compressive Differential Stress in Basin Interior, MPa
1	Imbrium-style	5	50	N	0
2		5	120	Y	−30
3		5	200	Y	−40
4	Flat floor	5	50	Y	−30
5		5	120	Y	−70
6		5	200	Y	−85
7		1 over 4	50	Y	−50
8		1 over 4	120	Y	−25
9		1 over 4	200	Y	−25

[a]Basin floor geometries are shown in Figure 2 (lower left inset). Fill thickness "1 over 4" refers to a 5-km-thick fill where the top 1 km was emplaced after subsidence associated with the bottom 4 km of fill had already been completed. The last column shows, for each case, the smallest compressive differential stress (maximum compressive stress minus minimum compressive stress) within the portion of the basin floor where ridges are observed (200 to 600 km from the basin center). Only case 1 violates the requirement that compressive differential stresses occur throughout this region.

for the remaining discussion of results, calculated stresses and predicted styles of faulting will be shown only for the top row of (1-km-thick) elements in the model.

[25] The case with the 50-km-thick lithosphere (case 1 in Table 1 and Figures 3a and 4a) leads to fairly small differential stresses in the outer regions of the basin where thrust faults are well developed (gray regions in Figure 3). Thus this combination of loading, basin floor geometry, and lithospheric thickness does not explain the distribution of thrust faulting seen in the basin interior. The case with the 120-km-thick lithosphere (case 2 in Table 1 and Figures 3b and 4b) predicts strike-slip faulting in the outer reaches of the observed thrust faulting region, though mixed-mode faulting could lead to surface features that resemble pure thrust faults. The case with the 200-km-thick lithosphere (case 3, Figures 3c and 4c) predicts thrust faults to 600 km radial distance (the outer reach of observed thrust faulting), with a differential stress of at least -40 MPa throughout the region.

[26] For the cases where the basin floor geometry remains flat to about 500 km radial distance from the basin center, subsidence associated with the extended thick load leads to compressional stresses farther from the basin center (cases 4, 5, and 6 in Table 1 and Figure 5). The result is pure thrust faulting throughout the region of observed contractional features and an increase of compressional stress by −30 MPa or more compared with the respective Imbrium-scaled floor geometry cases. Thus the continuation of thrust faults nearly to the outer edge of the basin floor suggests a relatively uniform load throughout most of the basin. A broader region of thick fill should lead to a broader gravity anomaly high (a broader mascon), which because of the northern latitude of Caloris should be observable by gravity mapping to be carried out by the MESSENGER mission.

[27] Stresses associated with the model for a broadly flat floor and a 50-km-thick lithosphere (case 4) are different from those for models with a thicker lithosphere (cases 5 and 6) in that for the latter cases the largest stresses are at the basin center, while the thinner-lithosphere case leads to stresses maximized at a distance of ~400 km from the basin center. This result, which simply reflects a lesser radial extent of deformation with a thinner lithosphere, is more nearly in line with the observation that ridges are most prominently developed outward of ~400 km radial distance. Imaging by MESSENGER of the entire basin floor, including the central regions, will help to discriminate among models.

[28] A 5-km-thick basin fill out to 500 km radial distance is a significant load, leading to significant compressive stresses in the basin that are difficult to overcome when exploring causes of later-stage normal faulting. Thus with the flat floor geometry, we also consider a model in which the upper 1 km of basin fill is not emplaced until subsidence associated with a lower 4-km-thick unit has already been completed. As with the single-stage fill model, only thrust faulting is predicted in the outer regions of the basin

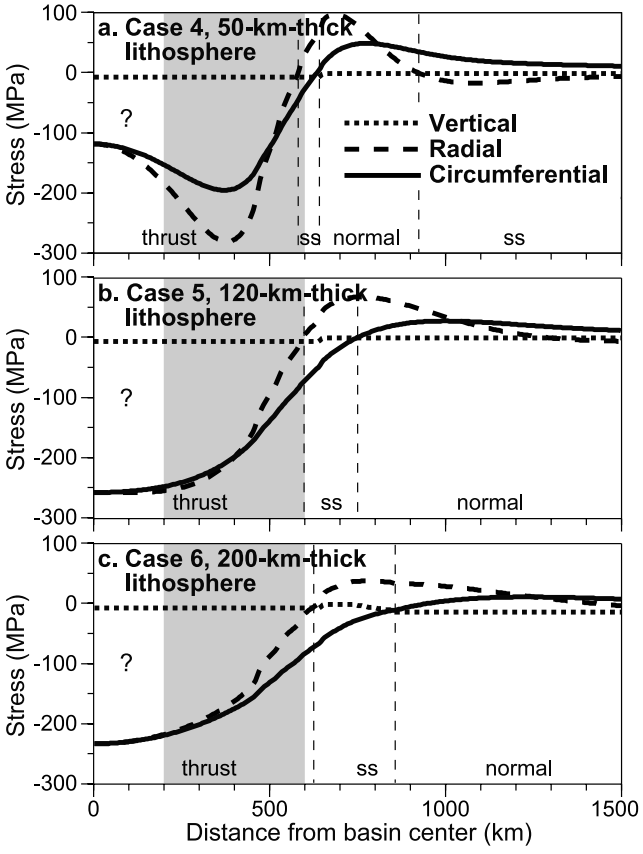

Figure 5. Same as Figure 3, but with a greater radial extent of basin floor at 5 km depth (dotted line in Figure 2, lower left inset). Case numbers refer to Table 1.

Table 2. Models for Later-Stage Normal Faulting Caused by Exterior Plains Emplacement[a]

Case	Interior Fill Thickness at Center, km	Lithospheric Thickness, km	Exterior Plains Thickness, km	Interior Normal Faults Predicted?	Smallest Differential Stress in 0–470 km range, MPa
10	5	50	1	N	−280
11	5	120	1	N	−230
12	5	200	1	N	−170
13	5	50	5	N	−220
14	5	120	5	N	−150
15	5	200	5	N	−70
16	5	50	10	N	−190
17	5	120	10	N	−50
18	5	200	10	Y	100
19	1 over 4	50	1	N	−30
20	1 over 4	120	1	N	−50
21	1 over 4	200	1	N	−10
22	1 over 4	50	5	N	30
23	1 over 4	120	5	Y	80
24	1 over 4	200	5	Y	90
25	1 over 4	50	10	Y	80
26	1 over 4	120	10	Y	200
27	1 over 4	200	10	Y	200

[a]Only flat floor geometries are considered (Figure 2, lower left inset). Fill thickness "1 over 4" refers to a 5-km-thick fill where the top 1 km was emplaced after subsidence induced by the lower 4 km of fill had already been completed. In order for a candidate model to predict normal faulting in the region where such features are most prominently observed, the smallest differential stress in this region (last column) must be at least +50 MPa, the estimated extensional stress equivalent to observed extensional strain.

(because of the flat floor geometry, the evolution of the fill does not greatly influence the shape of the radial variation of subsidence). However, the two-stage scenario leads to reduced compressional stresses in the top layer, as that layer experiences flexural stresses due to subsidence induced only by its own emplacement (cases 7, 8, 9 in Table 1). For the thicker-lithosphere cases, compressional differential stresses are as low in magnitude as −25 MPa within the region

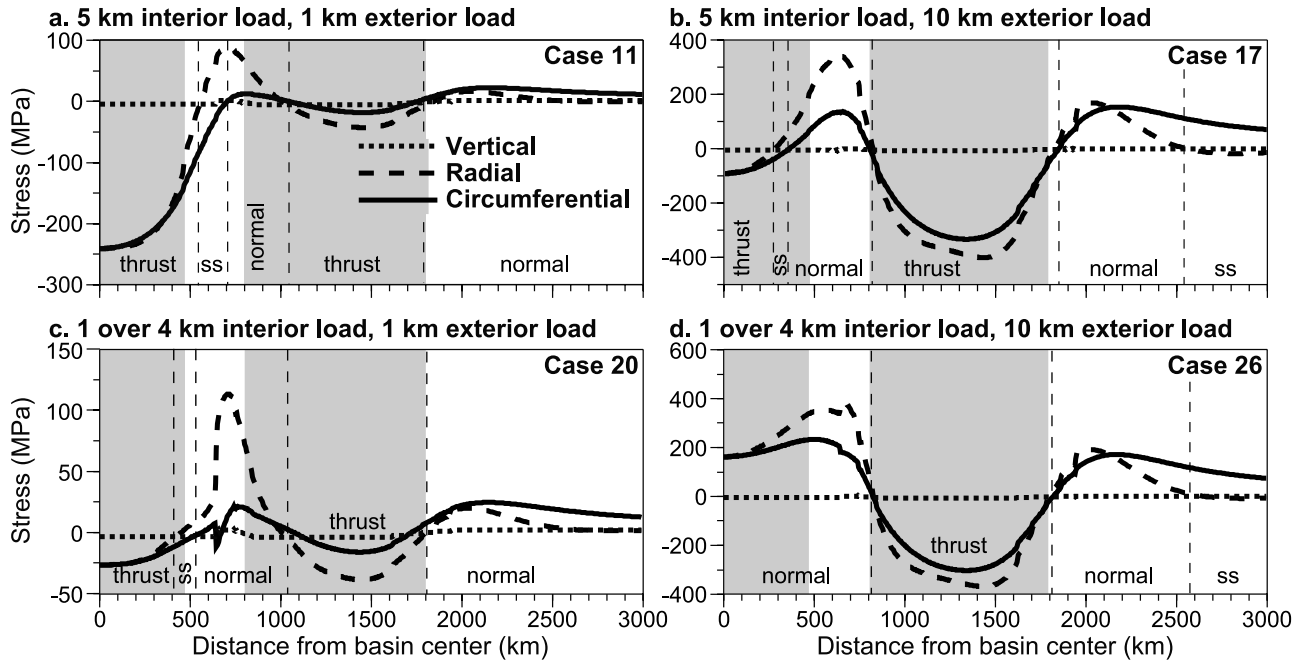

Figure 6. Principal stresses as functions of distance from the center of the Caloris basin after an initial stage of loading by basin fill and a later stage of exterior loading by annular smooth plains. All cases shown here have a flat floor geometry and a 120-km-thick lithosphere. Case numbers refer to Table 2. The "1 over 4 km interior load" refers to the case where the top 1 km of fill is emplaced after the subsidence induced by the emplacement of 4 km of fill has been completed. Negative stresses are compressive. The gray region on the left in each panel shows where later-stage normal faulting of the Caloris basin floor is observed to be most prominent (within 470 km of the basin center). The gray region on the right in each panel shows where compressional faulting outside the Caloris basin is observed (∼750–1800 km from the basin center).

where thrust faults are observed (Table 1). The magnitude of differential stress consistent with observed thrust faulting in the basin is not known, but the extension associated with observed normal faulting is equivalent to an extensional stress of about 50 MPa [*Watters et al.*, 2005]. If the same differential stress magnitude is needed for thrust faulting, then a thinner lithosphere (50 km thick) at the time of basin filling provides such a magnitude. However, compressional stress magnitudes toward the outer regions of the basin can be increased if the basin fill remains of similar thickness beyond even 500 km from the center. Again, gravity measurements by MESSENGER should prove useful in constraining fill geometry.

[29] Another factor that potentially could have influenced thrust faulting within the Caloris basin is that of global contraction caused by cooling of the planetary interior, which would have biased the two horizontal principal stresses toward compression. However, the global contractional stress that could influence this faulting is only that which arose during the window of time between partial infilling of the basin and the onset of the later-stage process that induced normal faulting. The cumulative contractional stress induced by global cooling over the entire preserved history of the planet has been inferred from the observed lengths and estimated throws of lobate scarps on the portions of Mercury well imaged by Mariner 10 [*Strom*, 1997; *Watters et al.*, 1998]. *Strom et al.* [1975], for example, estimated a 6.3×10^4 to 1.3×10^5 km^2 decrease in surface area, which corresponds to a decrease in planetary radius of 1-2 km. This decrease is equivalent to a contractional strain of 0.05–0.1%, which, with a Young's Modulus of 10^{11} GPa, suggests a cumulative compressional stress of −50 to −100 MPa. Since only a small fraction of this stress would be available to influence basin thrust faults in the aforementioned time window, it is not likely that global contraction had a significant influence on early-stage thrust faulting within the Caloris basin.

6. Second-Stage Exterior Loading

[30] The crosscutting of thrust faults by extensional troughs on the floor of the Caloris basin indicates a second stage of loading that reversed a compressional environment to one of horizontal extension. One of the scenarios to account for later-stage normal faulting on the basin floor is loading by an annulus of exterior smooth plains deposits that induced uplift of the basin interior by lithospheric flexure [*McKinnon*, 1980; *Melosh and McKinnon*, 1988]. To explore this scenario we use the flat basin floor geometry. For each model we first repeat the subsidence calculation to determine the state of stress prior to emplacement of the exterior load, then we introduce the exterior load and allow the asthenosphere to relax. In order for a candidate scenario to lead to predicted later-stage normal faulting, the net stress within the basin must be extensional in order to explain the development of normal faults, particularly within 470 km radial distance from the basin center. Table 2 summarizes the model configurations studied and the minimum extensional stress resolved in the region of most pronounced normal faulting.

[31] The stresses associated with the net response to an initial stage of loading by basin fill followed by a later stage of loading by external smooth plains are shown in Figure 6. The cases shown, which are all for a 120-km-thick lithosphere, demonstrate how stresses vary as functions of the size of the respective loads. In all cases the exterior annular loads lead to second-stage uplift of the basin and an increment of extension. However, in many cases this extension is insufficient to generate a net extensional environment in the basin (i.e., overcome the initial compressional stress state) and therefore fails to predict normal faulting. For example, Figures 6a and 6b show net stresses for cases where initial subsidence was due to a single-stage 5-km-thick interior load. This subsidence led to significant levels of compressional stress in the region of observed normal faulting (up to 470 km from the basin center) that could not be completely overcome even by a 10-km-thick external load (Figure 6b). Compression associated with two-stage basin fill was still too great to be overcome by a 1-km-thick external load (Figure 6c). However, two-stage interior filling followed by a 10-km-thick external load is able to induce extensional stresses in the area of observed normal faulting (Figure 6d).

[32] The extensional strain within the Caloris basin is estimated to be equivalent to ~50 MPa of extensional stress [*Watters et al.*, 2005]. As shown in Table 2, several cases lead to net extensional stresses in excess of this magnitude throughout the region of observed normal faulting. For the single-stage 5-km interior fill cases, only a 10-km-thick exterior load combined with a 200-km-thick lithosphere (case 18) satisfies this magnitude threshold. This threshold is satisfied by all two-stage interior fill cases with an exterior load of at least 5 km thickness (cases 23–27), except for the case with a 5-km-thick exterior load and only a 50-km-thick lithosphere (case 22).

[33] The stress states shown in Figure 6 are consistent with the observed orientation of normal faulting in Caloris basin. More than 200 km from the basin center the radial stress is predicted to be more positive than the circumferential stress. This is consistent with the observation by Mariner 10 of predominately circumferentially oriented graben in the outer basin. Within 200 km of the basin center the radial and circumferential stresses are predicted to be of similar magnitude, so that neither a radial nor circumferential orientation is preferred. One possible means for imparting a predominantly radial orientation would be that the 40-km-diameter impact crater at the center of the radial pattern of graben observed by MESSENGER [*Murchie et al.*, 2008] relieved extensional stress within the excavated region, which would lead to a radially outward movement of Caloris floor material, a decrease in the extensional radial stress, and an increase in the circumferential stress outward of the crater.

[34] Another factor that may come into play is the amount of compressional stress associated with initial basin subsidence that was relieved by early stage thrust faulting. If this stress relief was as great as 25–50 MPa, then the net stress after emplacement of the external load would have been that much higher (i.e., more extensional). In such a situation, all of the scenarios involving a multistage basin fill (cases 19–27 in Table 2) would predict later-stage normal faulting where such features are observed. A more detailed view of the topographic relief and extent of thrust faulting in the basin from future MESSENGER observations should en-

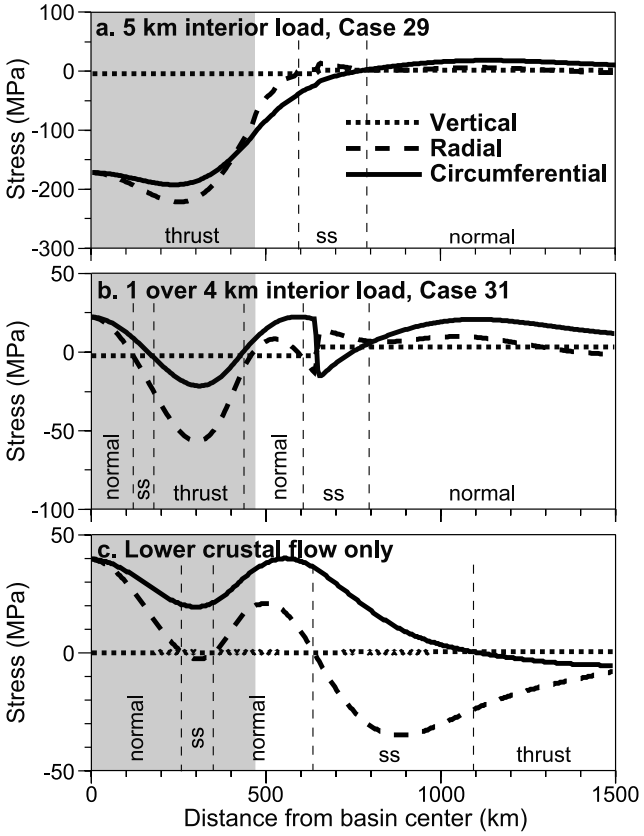

Figure 7. Principal stresses as functions of distance from the center of the Caloris basin associated with flexure in response to a later stage of lower crustal flow following initial basin subsidence. Both cases (a) and (b) are for a 200-km-thick lithosphere (see Table 3). The interior load thickness provided in each panel is the thickness at the center of a basin having a flat floor geometry (Figure 2, lower left inset). The "1 over 4 km interior load" in (b) refers to the case where the top 1 km of fill is emplaced after subsidence due to 4 km of fill has already occurred. Figure 7c shows principal stresses due to later-stage lower crustal flow only (after removal of all stresses associated with early subsidence). Negative stresses are compressive. The gray region shows the location where later-stage normal faulting in the Caloris basin is observed.

able some constraints to be placed on the extent of stress relief by faulting.

[35] The ability of an external annular load to induce thrust faulting where observed outside the basin (~750–1800 km from the basin center) is most dependent on the thickness of the external load. Figures 6a and 6c show that subsidence associated with a 1-km-thick external load is sufficient to induce compression within the load, but the differential stress magnitudes are less than −50 MPa, a level that may not account for the observed strain. However, if a significant portion of the estimated −50 to −100 MPa of compressional stresses associated with global contraction were added after the external smooth plains were emplaced, the combination of local and global contraction could readily have induced exterior thrust faulting. A 10-km-thick exterior load, in contrast, induces several hundred MPa of compression (Figures 6b and 6d) and could account for observed thrust faulting in the 750–1800 km radial distance range without the need for additional compression accompanying global contraction.

[36] Another consideration regarding the plausibility of an external load as the cause of extension within the basin and compression outside is whether such a load is topographically plausible. Our models show that placing external annular loads on 50-, 120-, and 200-km-thick lithospheres leads to subsidence of approximately 90%, 80%, and 60% of the load thickness, respectively. Radar altimetric profiles show that the surface of smooth plains units to the southeast of the Caloris basin is down-bowed by as much as 1 km relative to surrounding terrain, and profiles of probable smooth plains units to the southwest of the basin suggest as much as 2.5 km of down-bowing [*Harmon et al.*, 1986]. These profiles are permissive of several kilometers of subsidence during and following emplacement of these annular smooth plains units, but only if the plains lavas erupted onto terrain that was topographically low prior to plains emplacement or if smooth plains material is denser than the average density of the underlying crust.

7. Second-Stage Lower Crustal Flow

[37] An alternate scenario for the formation of later-stage extensional features within the Caloris basin is lateral flow of a viscoelastic lower crust [*Watters et al.*, 2005]. Flow arises from the horizontal pressure gradient associated with thinner crust beneath the basin than beneath surrounding regions. This scenario is based on the premise that the viscosity of the lower crust is sufficiently greater than the viscosity of the asthenosphere that subsidence induced by early-stage basin fill would be complete before significant lower crustal flow had initiated. Only in this manner could lower crustal flow drive a later stage of uplift and extension of the basin floor.

[38] In our simulations we adopted the same thicknesses of crust exterior to the basin (120 km) and viscoelastic lower crust (70 km) as in the analysis of *Watters et al.* [2005], values that likely maximize the influence of lower crustal flow on surface stresses. We utilized the flat basin floor geometries with lithospheric thicknesses of 120 and 200 km (the 50-km-thick lithospheric case is not relevant inasmuch as the lower crust would be part of the asthenosphere). In all cases later-stage lower crustal flow leads to uplift of the basin, but the associated extensional stresses are insufficient within a significant portion of the region of observed normal faulting (up to 470 km from the basin center) to overcome compressional stresses remaining after early-stage basin subsidence (Table 3). Net stresses following lower crustal flow for cases where the lithosphere is 200 km thick are shown in Figure 7. With an early single-stage 5 km of interior fill, subsequent lower crustal flow is insufficient to bring any portion of the basin interior into extension (Figure 7a). With an early two-stage basin fill, the basin center and edges can be brought into extension by subsequent lower crustal flow, but not the region where normal faults are most prominently observed (Figure 7b).

[39] The models described above do not take into account the fact that early stage thrust faulting relieved at least some fraction of compressional stresses induced by early subsidence. If the initial compressive stress state due to subsi-

Table 3. Models for Later-Stage Normal Faulting Caused by Lower Crustal Flow[a]

Case	Interior Fill Thickness at Center, km	Lithospheric Thickness, km	Interior Normal Faults Predicted?	Smallest Differential Stress in 0–470 km Range, MPa
28	5	120	N	−280
29	5	200	N	−220
30	1 over 4	120	N	−120
31	1 over 4	200	N	−60

[a]Only flat floor geometries are considered (Figure 2, lower left inset). Fill thickness "1 over 4" refers to a 5-km-thick fill where the top 1 km was emplaced after subsidence induced by the lower 4 km of fill had already been completed. In order for a candidate model to predict normal faulting in the region where they are most prominently observed, the smallest differential stress in this region (last column) must be at least +50 MPa, the estimated extensional elastic stress equivalent to observed extensional strain.

dence were completely relieved by thrust faulting, for our model with a 120-km-thick lithosphere, later-stage lower crustal flow would lead to significant extensional stresses in the innermost 300 km of the basin. Such a model leads to compressive stresses in the outer regions of the basin, however, and is thus not consistent with the observation that normal faulting extended to a distance of 470 km from the basin center. If the initial compressive stress state due to subsidence were completely relieved by thrust faulting and if the lithosphere were 200 km thick, our results indicate that later-stage lower crustal flow would lead to extension throughout the basin (Figure 7c). A problem with this scenario, however, is that such a model would predict normal faulting as well in the outermost basin (470–650 km from the basin center), where such features are not observed. We found no lithospheric thickness that would lead to normal faulting within 470 km distance of the basin center without also predicting their occurrence outward of this region. This outcome is due to the double maxima in the horizontal stress curves shown in Figure 7c. Changing the lithospheric thickness modifies the wavelength of this response but not the basic shape. We conclude that none of the lower crustal flow scenarios modeled here can explain the pattern of normal faulting observed in the Caloris basin.

[40] It is interesting to note that our predicted stress distribution due to lower crustal flow (Figure 7c) is significantly different from that of *Watters et al.* [2005], who suggest an inner extensional and an outer compressional lobe over the radial extent of the basin. This difference in stress patterns is perhaps not surprising considering the differences in the respective assumptions underlying their models and ours, including the geometry of the basin floor and fill, the elastic thickness, and particularly the assumption of isostasy prior to the onset of lower crustal flow adopted by *Watters et al.* [2005]. Our numerical approach enables us to consider the stress state accompanying lower crustal flow initiated from a nonisostatic configuration following initial basin subsidence. This configuration plays an important role, for example, in the double maxima in the stress distribution (Figure 7c) for our solution.

8. Summary and Conclusions

[41] Through a series of axisymmetric finite element models we have tested a range of models of lithospheric structure and surface loading in an effort to distinguish among scenarios put forward to explain the patterns of faulting observed within and exterior to the 1300-km-diameter Caloris basin on Mercury. The models support the inference that contractional features on the basin floor are consistent with subsidence associated with a flexural response to partial basin infilling by smooth plains deposits, presumed to be volcanic in origin. Models that account for the locations of contractional features near the edges of the basin floor involve fill that is of nearly uniform thickness over most of the basin (out to 500 km or greater distance from the basin center). This result suggests that the prefill Caloris basin floor was flatter than the geometry that has been inferred for similar sized basins on the Moon. A variety of fill thicknesses, emplacement scenarios, and lithospheric thicknesses lead to interior thrust faulting associated with subsidence. The observed distribution of contractional features is best matched by comparatively large values of fill thickness (several kilometers or more) but provides little constraint on lithospheric thickness.

[42] A later stage of normal faulting within the basin interior can be explained by the emplacement of exterior smooth plains within an annular zone that extends from 1 to 3 basin radii (750 to 1800 km) from the basin center. In order that flexural uplift within the basin induced by this external load modified the stress field beneath the basin floor from a state of compression to one of net extension, the external load must have been relatively thick (5 km or more). In addition, infilling of the basin floor must have occurred in stages spaced over a time frame longer than the timescale for basin subsidence in response to a single interior load, so as to reduce the early compressive stresses in the uppermost layer of basin-floor fill. Calculations show that later-stage flow of a viscous layer at the base of the crust can induce uplift of the basin, but not net extension, as early stage compressive stresses associated with basin subsidence are too great to be overcome. If, however, initial compressive stresses were completely relieved by thrust faulting, then a later-stage inward flow of the lower crust could, under some conditions, induce extension in the basin, though still not in a manner consistent with the observed distribution of normal faulting. Thrust faulting observed on exterior smooth plains can be the result of local loading-induced subsidence, again if these plains are relatively thick, but any constraint on the thickness of annular smooth plains from the distribution of exterior ridges can be substantially relaxed if significant compressional stresses associated with global contraction were superimposed.

[43] These results have implications for measurements of Mercury's gravity field to be obtained by the MESSENGER

mission. Because the models of this paper suggest that the formation of later-stage normal faults within the Caloris basin floor reflected primarily the near-surface stress state within only a surficial layer of fill material, the net displacement of the basin floor after all loading processes were completed was one of subsidence. If the freshly formed basin achieved a state of isostatic equilibrium prior to initial infilling, the Caloris basin interior should be the site of a positive free air gravity anomaly, i.e., a mascon. This inference is in contrast to the prediction of *Melosh and Dzurisin* [1978], who suggested that interior uplift should not occur if the basin floor has a net positive gravity anomaly. If interior uplift was the result of loading by exterior plains deposits, then basin floor uplift could have occurred even if the basin is a mascon. As *Melosh and Dzurisin* [1978] predicted, the exterior deposits should also be sites of positive gravity anomalies. The overall gravity anomaly associated with the basin and its surroundings might therefore be approximately that of a bull's-eye, with a central positive anomaly surrounded by a positive annulus separated from the central anomaly by a ring of lower gravity. The actual pattern, of course, is likely to be more complicated, reflecting departures from early local isostasy and uneven deposition of smooth plains deposits.

[44] The results of the models of this paper demonstrate that three of the most important factors that influenced faulting in and around the Caloris basin were the thickness and distribution of fill within the basin, the thickness of the exterior smooth plains deposits, and the amount of stress relief within the basin that accompanied early stage thrust faulting. The MESSENGER mission will obtain measurements of topography, gravity, and detailed fault characteristics that should substantially improve constraints on all of these factors, an outcome that will strengthen the importance of the Caloris basin as a laboratory for understanding interior heat flow, magmatism, and deformation during the early history of Mercury.

[45] **Acknowledgments.** This research was partially supported by the NASA Planetary Geology and Geophysics Program under grant NNG04GI64G. We thank Patrick McGovern, Francis Nimmo, and an anonymous reviewer for helpful reviews of an earlier draft.

References

Anderson, E. M. (1951), *The Dynamics of Faulting*, 206 pp., Oliver and Boyd, Edinburgh.

DeHon, R. A. (1979), Preliminary thickness study of plains-forming materials in the Caloris basin region of Mercury (abstract), in *Reports of Planetary Geology Program, 1978-1979, NASA TM-80339*, pp. 65–67, NASA, Washington, DC.

Dzurisin, D. (1978), The tectonic and volcanic history of Mercury as inferred from studies of scarps, ridges, troughs, and other lineaments, *J. Geophys. Res.*, *83*, 4883–4906.

Freed, A. M., H. J. Melosh, and S. C. Solomon (2001), Tectonics of mascon loading: Resolution of the strike-slip faulting paradox, *J. Geophys. Res.*, *106*, 20,603–20,620.

Hapke, B., G. E. Danielson Jr., K. Klaasen, and L. Wilson (1975), Photometric observations of Mercury from Mariner 10, *J. Geophys. Res.*, *80*, 2431–2443.

Harmon, J. K., D. B. Campbell, D. L. Bindschadler, J. W. Head, and I. I. Shapiro (1986), Radar altimetry of Mercury: A preliminary analysis, *J. Geophys. Res.*, *91*, 385–401.

Head, J. W. (1974), Orientale multi-ringed basin interior and implications for the petrogenesis of lunar highland samples, *Moon*, *11*, 327–356.

Kiefer, W. S., and B. C. Murray (1987), The formation of Mercury's smooth plains, *Icarus*, *72*, 477–491.

McKinnon, W. B. (1980), Large impact craters and basins: Mechanics of syngenetic and postgenetic modification, Ph.D. thesis, California Inst. of Technol., Pasadena, Calif.

McKinnon, W. B. (1986), Tectonics of Caloris basin, Mercury, paper presented at Mercury Conference, Div. Planet. Sci. Amer. Astron. Soc. and Intl. Astron. Union Comm. 16, Tucson, Ariz., 6–9 August.

Melosh, H. J. (1978), Tectonics of mascon loading, *Proc. Lunar Planet. Sci. Conf. 9th*, 3513–3525.

Melosh, H. J., and D. Dzurisin (1978), Tectonic implications for the gravity structure of Caloris basin, Mercury, *Icarus*, *33*, 141–144.

Melosh, H. J., and W. B. McKinnon (1988), The tectonics of Mercury, in *Mercury*, edited by F. Vilas, C. R. Chapman, and M. S. Matthews, pp. 374–400, Univ. of Arizona Press, Tucson, Ariz.

Melosh, H. J., and A. Raefsky (1980), The dynamic origin of subduction zone topography, *Geophys. J. R. Astron. Soc.*, *60*, 333–354.

Murchie, S. L., et al. (2008), Geology of the Caloris Basin, Mercury: A view from MESSENGER, *Science*, *231*, 73–76.

Nimmo, F., and T. R. Watters (2004), Depth of faulting on Mercury: Implications for heat flux and crustal and effective elastic thickness, *Geophys. Res. Lett.*, *31*, L02701, doi:10.1029/2003GL018847.

Pechman, J. C. (1980), The origin of polygonal troughs on the northern plains of Mars, *Icarus*, *42*, 185–210.

Peltier, W. R. (2004), Global glacial isostasy and the surface of the ice-age Earth: The ICE-5G (VM2) model and GRACE, *Annu. Rev. Earth Planet. Sci.*, *32*, 111–149.

Phillips, R. J., J. E. Conel, E. A. Abbott, W. L. Sjogren, and J. G. Morton (1972), Mascons: Progress toward a unique solution for mass distribution, *J. Geophys. Res.*, *77*, 7106–7114.

Pike, R. J. (1988), Geomorphology of impact craters on Mercury, in *Mercury*, edited by F. Vilas, C. R. Chapman, and M. S. Matthews, pp. 165–273, Univ. of Arizona Press, Tucson, Ariz.

Solomon, S. C. (2003), Mercury: The enigmatic innermost planet, *Earth Planet. Sci. Lett.*, *216*, 441–455.

Solomon, S. C., and J. W. Head (1979), Vertical movement in mare basins: Relation to mare emplacement, basin tectonics, and lunar thermal history, *J. Geophys. Res.*, *84*, 1667–1682.

Solomon, S. C., and J. W. Head (1980), Lunar mascon basins: Lava filling, tectonics, and evolution of the lithosphere, *Rev. Geophys.*, *18*, 107–141.

Solomon, S. C., et al. (2001), The MESSENGER mission to Mercury: Scientific objectives and implementation, *Planet. Space Sci.*, *49*, 1445–1465.

Solomon, S. C., R. L. McNutt Jr., R. E. Gold, and D. L. Domingue (2007), MESSENGER mission overview, *Space Sci. Rev.*, *131*, 3–39.

Spudis, P. D., and J. E. Guest (1988), Stratigraphy and geologic history of Mercury, in *Mercury*, edited by F. Vilas, C. R. Chapman, and M. S. Matthews, pp. 118–164, Univ. of Arizona Press, Tucson, Ariz.

Strom, R. G. (1984), Mercury, in *The Geology of the Terrestrial Planets*, edited by M. H. Carr, NASA SP-469, pp. 13–55, NASA, Washington, DC.

Strom, R. G. (1997), Mercury: An overview, *Adv. Space Res.*, *19*, 1471–1485.

Strom, R. G., N. J. Trask, and J. E. Guest (1975), Tectonism and volcanism on Mercury, *J. Geophys. Res.*, *80*, 2478–2507.

Watters, T. R., M. S. Robinson, and A. C. Cook (1998), Topography of lobate scarps on Mercury: New constraints on the planet's contraction, *Geology*, *26*, 991–994.

Watters, T. R., F. Nimmo, and M. S. Robinson (2005), Extensional troughs in the Caloris basin of Mercury: Evidence of lateral crustal flow, *Geology*, *33*, 669–672.

Williams, K. K., and M. T. Zuber (1998), Measurement and analysis of lunar basin depths from Clementine altimetry, *Icarus*, *131*, 107–122.

A. M. Freed and P. J. Kennedy, Department of Earth and Atmospheric Sciences, Purdue University, 550 Stadium Mall Drive, West Lafayette, IN 47907, USA. (freed@purdue.edu)

S. C. Solomon, Department of Terrestrial Magnetism, Carnegie Institution of Washington, 5241 Broad Branch Road, N.W., Washington, DC 20015, USA. (scs@dtm.ciw.edu)